Nuclear Instruments and Methods in Physics Research B31 (1988) 336–341
North-Holland, Amsterdam

"SADDLE-POINT" IONIZATION

T.J. GAY, H.G. BERRY [1], E.B. HALE, V.D. IRBY and R.E. OLSON

Laboratory for Atomic and Molecular Research and
Physics Department, University of Missouri-Rolla Rolla, MO 65401, USA
[1] *Physics Division, Argonne National Laboratory, Argonne, IL 60439, USA*

We have studied the ionization of rare gases by protons at intermediate energies, i.e., energies at which the velocities of the proton and the target-gas valence electrons are comparable. A significant channel for electron production in the forward direction is shown to be "saddle-point" ionization, in which electrons are stranded on or near the saddle-point of electric potential between the receding projectile and the ionized target. Such electrons yield characteristic energy spectra, and contribute significantly to forward-electron-production cross sections. Classical trajectory Monte Carlo calculations are found to provide qualitative agreement with our measurements and the earlier measurements of Rudd and coworkers, and reproduce, in detail, the features of the general ionization spectra.

1. Introduction

In ion–atom ionizing collisions, a standard picture has developed over the last twenty years, in which the ionized electron is associated either with the target, as in the case of target autoionization or simple impulsive "direct" ionization, or with the projectile, as in the case of charge-transfer to the continuum (CTC). Historically, this view would appear to have arisen because of the general, monotonic decrease with energy of singly-differential electron spectra, and the striking nature of the CTC cusp in doubly-differential energy spectra taken at 0°. Moreover, this picture is prompted by a simple classical view of the ionization process: ionized electrons will tend to fall into one of the two Coulomb wells formed by the ionized target and the receding projectile, and can thus naturally be associated with one of the two charge centers.

Departures from this standard picture have begun to appear in the last several years. In 1983, in classical trajectory Monte Carlo (CTMC) studies of the ionization of atomic hydrogen by protons, Olson observed a significant enhancement of electrons with velocities close to $V_p/2$, where V_p is the velocity of the projectile after the collision [1]. He attributed this enhancement to the "stranding" of electrons in the region of little or no electric field corresponding to the the saddle-point region of the electric potential between the two charge centers. More recently, Winter and Lin, studying the same system at lower energies with close-coupling calculations, found that a significant improvement between their predictions and experimental results was attained by inclusion of basis states centered at the midpoint between the two protons [2]. Implicit in this improvement is the existence of a significant number of ionized electrons with velocities comparable to $V_p/2$. Recently, a number of authors have discussed several points with regard to the three-body nature of ionizing collisions and problems associated with our understanding of forward-electron emission in ionizing collisions [3–7].

In this paper we present measurements of proton–rare-gas ionization spectra which elucidate the nature of ionized-electron emission in the forward direction. In particular, we have observed significant "saddle-point" ionization, in which the electron is pulled from the target by the receding proton, and is left stranded on or near the saddle point of electric potential. The saddle point electrons are a global phenomenon which make a large contribution to total ionization cross sections at intermediate (~ 100 keV) energies. The importance of this mechanism is shown clearly by our CTMC calculations, which are in good agreement both with our measurements and those of Rudd and coworkers [8–10].

2. Experimental procedure

In the experiments that we performed, proton beams impinged on an effusive gas target, and ionized electrons were detected at specific angles following passage through an electrostatic analyzer [11]. The proton beams were produced in either a Colutron or a microwave-discharge ion source. Following acceleration and mass selection, the beam was tightly collimated ($\Delta\theta < 3$ mrad) prior to entering a mu-metal shielded target chamber, where residual magnetic fields were reduced to less than 0.5 μT. The beam then traversed an effusive target, produced by a vertical metal capillary tube, situated

0168-583X/88/$03.50

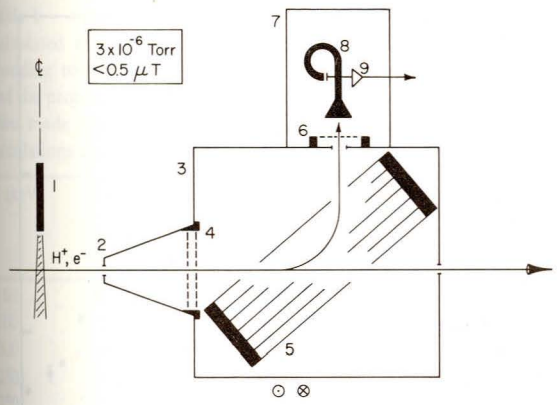

Fig. 1. Schematic drawing of the rotatable electrostatic analyzer housing. The 0° configuration is shown, in which both the incident protons and secondary electrons pass through the analyzer. Shown are 1) target capillary; 2) entrance collimator; 3) brass sheet housing; 4) fine mesh grids to provide for acceleration or deceleration of the electron beam prior to entering the deflection region (not used in our experiment); 5) parallel plate analyzer with fringe-field plates; 6) fine mesh grid for acceleration of electrons into channeltron; 7) channeltron housing; 8) channeltron; 9) charge-sensitive preamp and signal out.

directly above the entrance to a 4 in. diffusion pump (see fig. 1). Typical background pressure in the chamber was 3×10^{-6} Torr.

Ionized electrons were detected by a channeltron after passing through a parallel-plate electrostatic analyzer. The analyzer was housed in a brass box which was in turn mounted on a rotatable arm, whose axis of rotation coincided with the axis of the target gas capillary tube. The analyzer could be rotated through an angular range (relative to the proton beam) of $\pm 120°$, although measurements were only possible at 0° (by virtue of large apertures in the front and back plate of the analyzer and its housing) and at angles between 17° and 120° (for angles $1° \lesssim \theta \lesssim 16°$, the analyzer housing geometrically obstructed the proton beam). The angular acceptance for electron detection was determined geometrically by the size of the channeltron entrance ($\pm 3°$ horizontally) and the width of the analyzer exit aperture ($\pm 1°$ vertically). The vertical acceptance was increased by the focussing properties of the analyzer, but was ultimately limited by the size of the housing entrance aperture, a 3.5 mm diameter hole located 2.3 cm from the center of the target. The proton beam current was measured with a deep Faraday cup.

Ionized electron energy spectra at specific angles were taken by sweeping the analyzer plate voltage and monitoring the analog signal from a ratemeter connected to the channeltron pulse-counting electronics. The results were recorded using an $X-Y$ recorder driven by the plate voltage (X-axis) and the ratemeter output (Y-axis). Typically, data were continuously taken as the plate voltage was swept back-and-forth twice with gas on and twice with gas off. Proton beam current fluctuations were easily kept below 5%. Typical beam currents were 20 nA, with electron count rates ranging from a few Hz to tens of kHz. Target gas density was monitored crudely by reading the chamber pressure. Most spectra were taken with a gauge reading of $\sim 1.5 \times 10^{-5}$ Torr. We estimate the pressure in the collision volume to be roughly 5 to 10 times the pressure read by our ionization gauge. Electron count rates were observed to depend linearly on pressure between 3×10^{-6} and 6×10^{-5} Torr at both 90° and 17°.

Analyzer performance was checked periodically by shooting a variable-energy beam of electrons, from an auxiliary electron gun in the chamber, into the analyzer. The system's energy resolution was about 10% and did not change with time. Also, the relationship between plate voltage and electron-pass energy remained constant, and, within error, always had a zero-intercept. Thus, we expect that effects due to changing contact potentials affect our results minimally.

Our energy spectra have been normalized in two ways. First, the relative detection efficiency vs. energy was periodically calibrated by measuring a He ionization spectrum at 150 keV at 30°, and then determining an "efficiency function" which, when multiplied by our raw data, yielded the published, smoothed values of Rudd and Jorgensen [8]. Subsequent data was put on an absolute scale by normalizing to interpolated, absolute, double-differential cross section values of Rudd et al. [8–10]. Absolute errors in our data are derived from the absolute errors discussed by Rudd and Madison [10]. Relative errors in individual spectra are typically 10%.

3. Results and discussion

Unambiguous observation of possible saddle point ionization can be complicated by projectile-centered ionization phenomena which dominate energy spectra taken at or near 0°. For this reason, we have made measurements at 17°, where projectile-centered effects will be negligible. A sample of ionized electron spectra, plotted in velocity space, is shown in fig. 2. A maximum in the cross section roughly midway between the projectile ($v_e/v_p = 1$) and target ($v_e/v_p = 0$) velocities is clearly seen at all projectile energies. We attribute these maxima to the saddle-point ionization mechanism. Our CTMC results for these doubly-differential spectra agree qualitatively with the measurements, both in shape and absolute magnitude. The relative velocities at which the spectra have a maximum decreases with increasing projectile energy in both the calculations and the measurements. Nonetheless, electrons with velocities in the middle third of the $v_e/v_p = 0$ to 1 range of these spectra

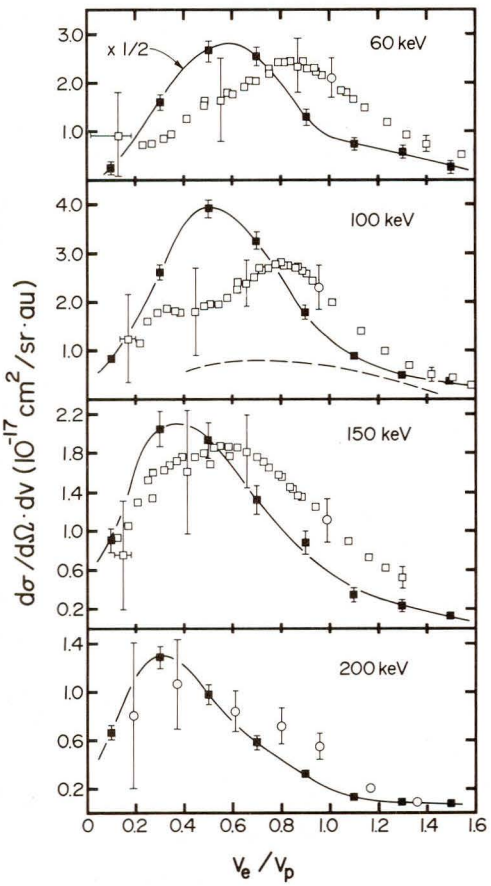

Fig. 2. Doubly-differential cross sections for electrons ejected at 17° for 60, 100, 150, and 200 keV incident protons on He targets. The electron velocities (v_e) are normalized to the projectile velocities (v_p). The filled squares are absolute values from our CTMC calculations. The solid lines serve to guide the eye. The dashed line is the prediction of a distorted-wave Born approximation calculation [10]. The open squares are our experimental data, normalized at $v_e \approx v_p$ to absolute values interpolated from the data of refs. [8] and [9] (open circles). The horizontal error bars represent uncertainty in velocity due to the effects of contact potentials.

make up a significant fraction of the total electron production. We have observed similar features with He and other rare gases at 17° as well as 25° (see, e.g., fig. 3).

As mentioned earlier, the problem with studying saddle point ionization near 0° is that projectile centered phenomena, e.g., CTC and transfer ionization (in which the proton captures two electrons into an autoionizing state of H^-) dominate the electron spectra at small angles [7]. This is illustrated in fig. 4 [10,12]. At 0°, the spectrum is completely dominated by CTC and other projectile-centered ionization at $v_e = v_p$ (27.2 eV), although the hint of a mid-point bump can be seen at

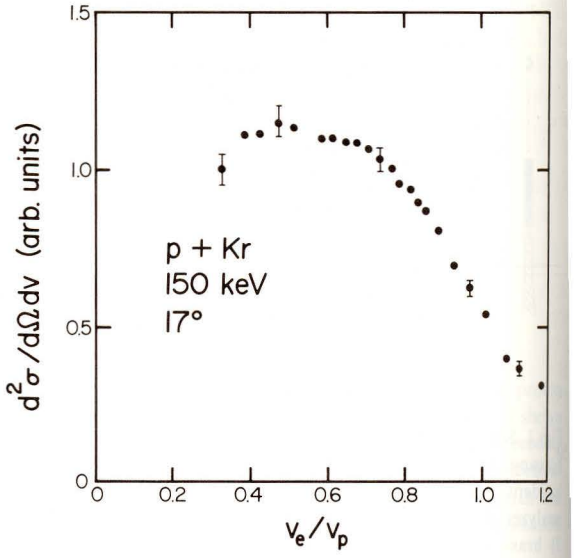

Fig. 3. Doubly-differential electron spectrum for electron ejection at 17° for $H^+ + Kr$. Error bars present relative uncertainty of the data. Velocity uncertainties are similar to those in fig. 2.

about 14 eV ($v_e/v_p = 0.72$). Projectile-centered electrons still affect the spectrum significantly at 5°, but the pure signature of the saddle-point bump is seen at 10°. By 20°, target centered (low-velocity) electrons are beginning to wash out the saddle-point maximum.

In order to complement these observations, we have calculated the fraction of electrons which fall into each of three bins following $H^+ + He$ ionizing collisions [7]. When the nuclei were 50 a.u. apart, the post-collision volume was divided into three regions to represent proximity to the target, the projectile, and the midpoint between the two. The boundaries of the regions were

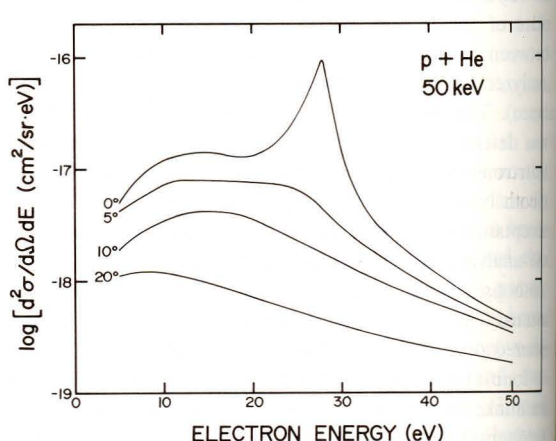

Fig. 4. Doubly-differential energy spectra of ionized electrons in $H^+ + He$ collisions. Data at 0°, 5°, and 10° are taken from figures in ref. [12]. The 20° data are from ref. [10].

Table 1
Calculated ejected-electron flux for the three regions corresponding to the target ion, the midpoint between the nuclei, and the projectile for $H^{\pm} + He$ collisions. Binning assignments were made when the nuclei were 50 a.u. apart. Antiproton calculations are in parentheses

E (keV)	Flux fraction (%)		
	Target region	Midpoint region	Projectile region
60	19.1 ± 0.9	57.8 ± 1.5	23.1 ± 1.0
100	24.5 ± 0.8	59.4 ± 1.3	16.1 ± 0.7
200	46.8 ± 1.4	47.6 ± 1.4	5.6 ± 0.5
(250)	(67.8 ± 2.8)	(31.8 ± 1.9)	(0.5 ± 0.2)
250	50.7 ± 2.1	45.9 ± 2.1	3.4 ± 0.5
300	61.1 ± 1.6	36.8 ± 1.3	2.1 ± 0.3
(500)	(80.5 ± 3.0)	(19.5 ± 1.5)	(–)
500	74.8 ± 2.0	24.6 ± 1.2	0.6 ± 0.2

$z = 50 \times 1/3$ a.u. and $z = 50 \times 2/3$ a.u., where z is parallel to the projectile velocity, and the target is assumed to be stationary at $z = 0$. The fractions of electrons in each bin are given in table 1. Convergence of these fractions was checked at an internuclear separation of 100 a.u. A surprising result is that electrons associated with the middle region actually dominate the total ionization cross section for energies up to 200 keV. The increasing importance of the target bin (and the attendant decrease of electrons in the projectile bin) with increasing projectile energy is consistent with our observation that the velocity position of the differential cross section maximum decreases with increasing projectile energy.

Of additional interest is the relative population of the mid-point bin when proton and antiproton projectiles are compared. In the antiproton case, of course, no saddle-point mechanism can be active. The enhancement of mid-point region electrons with proton projectiles can be taken as further evidence for, and a measure of the importance of, the saddle-point mechanism at 250 and 500 keV. Calculations for lower energy antiproton collisions are in progress. We note that at both 250 and 500 keV, the cross sections for production of electrons in the first bin are the same, within error, for both projectiles. The difference in the total ionization cross sections for protons vs antiprotons is due almost entirely to differences in the mid-point flux.

The general quality of the CTMC calculations is illustrated in fig. 5, where they are compared with measured doubly-differential $H^+ + He$ ionization cross sections plotted vs ejection angle [7,10]. While the Born calculations are inadequate to describe the ionization, CTMC predictions are in good agreement with the measurements at all energies and angles, including the low-angle, 54.4 eV CTC cusp.

Additional evidence for the saddle-point mechanism

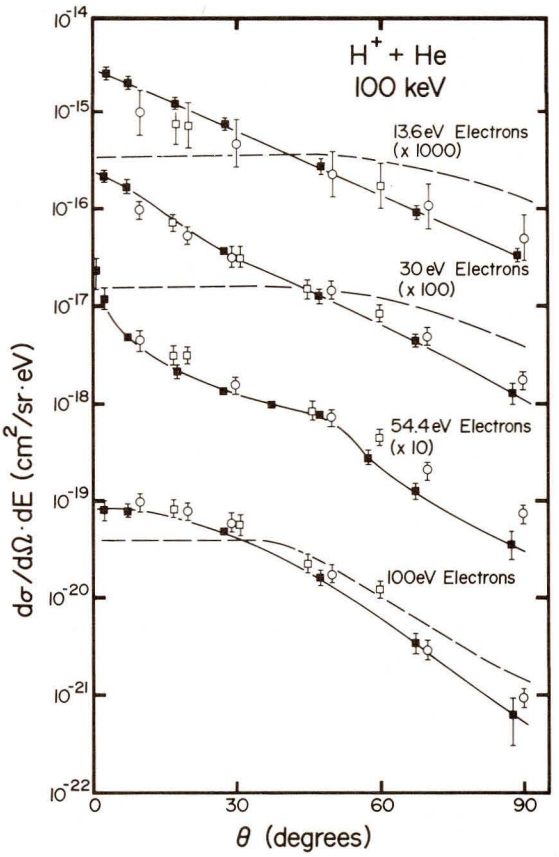

Fig. 5. Doubly-differential ionization cross sections vs ejection angle for 100 keV $H^+ + He$. The filled squares are absolute values from our CTMC calculations. The open squares are our experimental data; the 13.6 and 54.4 eV points are normalized to interpolated values from ref. [8] at 30°. The 30 and 100 eV data are normalized to values from ref. 10 at 20°. The open circles are absolute cross sections from ref. [9] and interpolated values from ref. [8]. The dashed lines are plane-wave Born calculations from refs. [9] and [10].

results from the comparison of ionization spectra for incident protons and electrons. We consider here 10° ejection from He bombarded by 200 keV protons [9] and 100 eV electrons [13], which have, within 4%, the same velocity. Because the incident electron experiments cannot distinguish between incident and target electrons in the exit channel, it is important, for purposes of comparison, to consider only low energy electrons, which come predominantly from the target. A comparison of the velocity spectra is shown in fig. 6. The scattered electron spectrum for incident electrons was terminated somewhat arbitrarily at 17.9 eV. The differential cross sections rise at higher energy due to the increasing importance of incident electrons in the spectrum. Again, the relatively weak mid-region ionization is evident in the electron case. We note the lack of a low velocity maximum (or even an obvious inflection

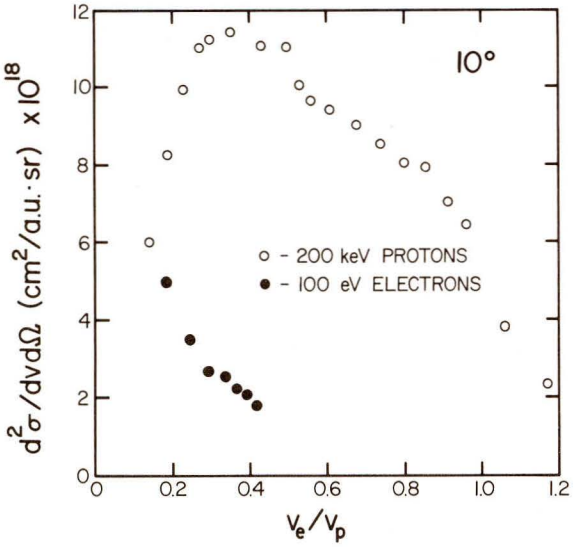

Fig. 6. Doubly-differential ionization cross sections for 10° ejection with 100 eV incident electrons and 200 keV incident protons. Data from refs. [9] and [13]. The relative uncertainty in the data is roughly 10% for incident protons and 25% for incident electrons.

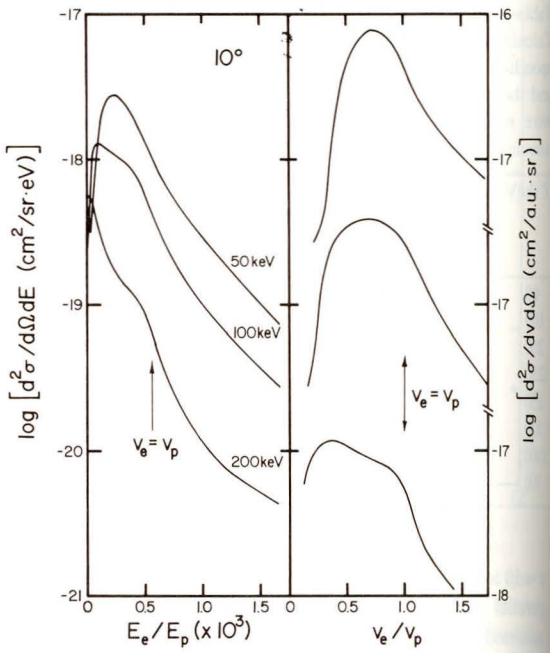

Fig. 7. Doubly-differential ionization spectra for $H^+ + He$ at 10° in both velocity and energy space. The data are from refs. [8] and [9]. The electron energies (E_e) have been normalized to the incident proton energy (E_p).

point) in the electron spectrum. This illustrates that plotting of data in velocity space need not yield a maximum. While maxima which occur in energy space are enhanced in velocity space (compare, e.g., fig. 2 and fig. 4), the saddle-point maximum is not, per se, an artifact of velocity space.

Although the intense interest in saddle-point electrons and the three-body nature of ionizing collisions is fairly recent [4,7], saddle-point ionization was first observed at small angle in 1963 by Rudd and Jorgensen [8], who noted that "the 'humps' on the 10° curves were thought to be due to spurious electrons, but reruns with additional shields failed to eliminate them". Subsequently, with the discovery of CTC, these features were explained routinely as being the shoulder of the cusp structure at 0° and $v_e/v_p = 1$. Contrary to this, we now understand these features to be the unambiguous signature of saddle-point ionization. Fig. 7 shows the 10° data for $H^+ + He$ of refs. [8] and [9] plotted both in velocity and energy space. The features in the energy spectra are enhanced in velocity space, but more importantly, they do not yield a peak at $v_e/v_p = 1.02$, where kinematically a peak resulting from simple CTC would occur.

In conclusion, we find saddle point ionization to be a global phenomenon, whose signature is the enhancement of electron production at small (~ 15°) angles in the forward direction at velocities comparable to half the projectile velocity. Our CTMC calculations show that electrons which include saddle-point electrons as a subset, namely the mid-region electrons, can actually account for a plurality of the ionized electrons at intermediate projectile energies (~ 100 keV) in $H^+ + He$ collisions. Perhaps surprisingly, these classical calculations yield in detail all of the general features of the ionization spectra.

The authors gratefully acknowledge the support of the USDOE (Office of Fusion Energy; V.D.I. and R.E.O., and the Office of Basic Energy Sciences; H.G.B.) and the Physics Divsion of the National Science Foundation (T.J.G.)

References

[1] R.E. Olson, Phys. Rev. A27 (1983) 1871.
[2] T.G. Winter and C.D. Lin, Phys. Rev. A29 (1984) 3071.
[3] R.E. Olson, Phys. Rev. A33 (1986) 4397.
[4] W. Meckbach, P.J. Focke, A.R. Goni, S. Suarez, J. Macek, and M.G. Menendez, Phys. Rev. Lett. 57 (1986) 1587.
[5] P. van der Straten, R. Morgenstern, and A. Niehaus, Abstracts of Contributed Papers to 15th Int. Conf. on the Physics of Electronic and Atomic Collisions, Brighton, England, (1987) p. 605.
[6] See e.g. M.G. Menendez and M.M. Duncan, Phys. Rev. A36 (1987) 1653.
[7] R.E. Olson, T.J. Gay, H.G. Berry, E.B. Hale, and V.D. Irby, Phys. Rev. Lett. 59 (1987) 36.

[8] M.E. Rudd and T. Jorgensen, Jr., Phys. Rev. 131 (1963) 666.
[9] M.E. Rudd, C.A. Sautter, and C.L. Bailey, Phys. Rev. 151 (1966) 20.
[10] M.E. Rudd and D.H. Madison, Phys. Rev. A14 (1976) 128.
[11] P.W. Arcuni, Ph.D. Thesis, University of Chicago (1985) (unpublished), and Phys. Rev. A33 (1986) 105.
[12] D.K. Gibson and I.D. Reid, J. Phys. B19 (1986) 3265.
[13] M.E. Rudd and R.D. Dubois, Phys. Rev. A16 (1977) 26.